Combination of Confocal Raman Spectroscopy and Electron Microscopy on the Same Individual Bundles of Single-Walled Carbon Nanotubes

ARTICLE *in* NANO LETTERS · SEPTEMBER 2002

Impact Factor: 13.59 · DOI: 10.1021/nl025738o

NANO LETTERS

2002
Vol. 2, No. 11
1209−1213

Combination of Confocal Raman Spectroscopy and Electron Microscopy on the Same Individual Bundles of Single-Walled Carbon Nanotubes

Chaoyang Jiang, Jixue Li, Jialong Zhao, Ute Kolb, and Alf Mews*

Institut für Physikalische Chemie, Universität Mainz, Mainz D-55099, Germany

Received August 7, 2002; Revised Manuscript Received August 30, 2002

ABSTRACT

We report a method to investigate the same individual single-walled carbon nanotube (SWNT) bundles with both transmission electron microscopy (TEM) and Raman spectroscopy. Free-standing individual bundles are obtained by depositing a solution of suspend SWNTs on a carbon film with a regular pattern of holes, which can be localized by TEM and also by confocal Raman microscopy. While most of the TEM images predict that the bundles consist of tubes with a similar diameter, we will show that occasionally a certain tube diameter can be associated with a particular radial breathing mode frequency of the Raman spectrum.

Single-walled carbon nanotubes (SWNTs) are one-dimensional molecular structures with diameters in the range of a few nanometers. The outstanding mechanical and electrical properties of these materials have generated significant activity in both fundamental and applied research.[1,2] For example, scanning probe tips[3] have been made using SWNTs because of their high mechanical strength. Also, the possibility of nanoscale electronic devices was shown by the realization of single-electron transistors made from SWNTs.[4,5]

In principle, a SWNT can be either metallic or semiconducting, depending on its diameter and chirality. Moreover, SWNTs made by arc-discharge[6] and laser ablation[7] methods usually self-tangle into bundles containing both metallic and semiconducting tubes. Therefore, the structural and electronic analysis of SWNT bundles is of great interest, particularly in the view of bundle applications.

The structural properties of individual bundles can be investigated by several microscopic techniques.[6−11] In cases of high resolution transmission electron microscopy (HR-TEM) it was even possible to directly observe cross sections of SWNT bundles when the bundle axis was perpendicular to the image plane. From these experiments it was argued that the triangular lattice of SWNT bundles is formed by nanotubes that are similar in diameter.[6,7] A powerful technique to probe the electronic properties of bundles and also individual SWNTs is the method of Raman microscopy and spectroscopy.[12−14] One of the features in a typical Raman spectrum of SWNTs is the radial breathing mode (RBM) in the region of 100−350 cm^{-1}. Because the RBM frequency is sensitive to the tube diameter and chirality,[12,15] a structural analysis of the SWNTs can also be performed by the method of Raman spectroscopy.

The relationship between the tube diameter d and the RBM frequency ω_{RBM} has been investigated by several groups and can, in principle, be described by the following formula:

$$d[\mathrm{nm}] = x/\omega_{RBM}[\mathrm{cm}^{-1}] \quad (1)$$

Bandow and co-authors used a force constant model and calculated a constant value of $x = 224$ independent of the chirality of the tubes.[16] Jorio et al.[17] used a combination of theory and Raman experiments where they could assign even the (n,m) chiral vector to individual SWNTs by using a parameter of $x = 248$. In addition, there have been many different ab initio calculations on the lattice dynamics of individual SWNTs and bundles. For example, Henrard et al. obtained that the expected RBM frequency is not independent of the tube chirality[11] and also predicted an upshift in frequency by 5−15% for tubes within bundles[18] (see also Figure 4). A possible bundle effect has also been reported by other groups.[19,20]

An experimental correlation between the frequency and diameter distributions of SWNT samples can, in principle, be performed by investigating the same set of samples with Raman spectroscopy and TEM or X-ray diffraction.[21,22] In this work we try to avoid averaging over the whole SWNT ensemble by investigating the same SWNTs with TEM and Raman spectroscopy. We present a method to directly correlate the structural and spectroscopic properties of

* Corresponding author. E-mail: alf.mews@mail.uni-mainz.de.

10.1021/nl025738o CCC: $22.00
Published on Web 09/28/2002

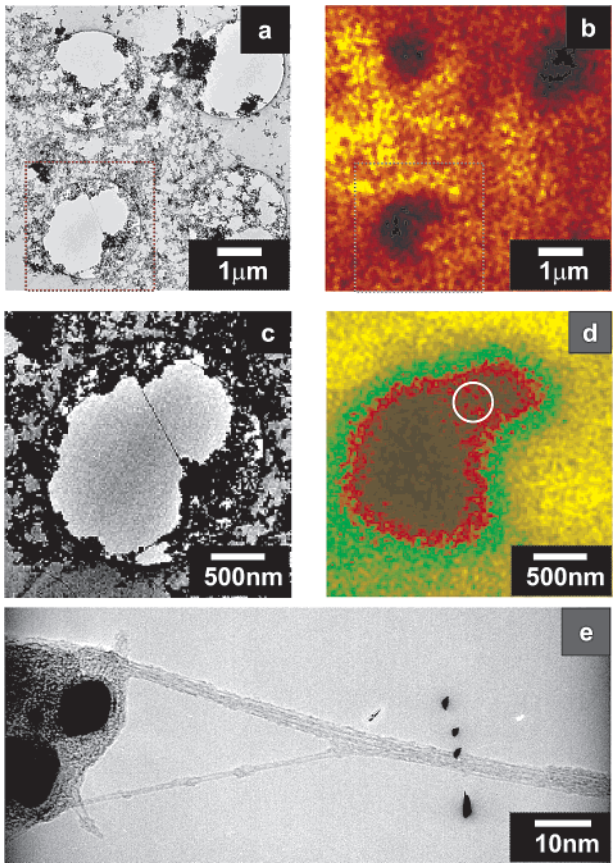

Figure 1. Localization of individual SWNT bundles in TEM and Raman experiments. (a) TEM image of SWNT raw material on a holey carbon film. (b) Raman G-line image of the same position as in (a). (c) Magnified area of (a) where the individual bundle across the hole is clearly observed by TEM. (d) Raman image of the same area as in (c). The circle indicates the spatial area from which a Raman spectrum can be obtained. (e) HRTEM image of the end of the free-standing bundle in (c). The bundle did not grow from a single catalyst particle and consists of at least two "sub-bundles".

identical SWNT bundles by comparing the TEM images and respective RBM Raman spectra of the same individual bundles.

To localize and investigate the same bundles in the different experiments, the choice of the substrate is of major importance. Here we used QUANTIFOIL carbon films, with a regular hole pattern that is supported by a Maxtaform Finder copper grid (Plano, W. Plannet GmbH), which allows to trace back the same holes in a TEM and a confocal scanning optical microscope. For sample preparation, a sonicated suspension of the SWNT raw material as produced by arc-discharge (Carbolex, Lexington, KY) in $CHCl_3$ was dropped on the holey carbon grid and allowed to evaporate. A low resolution TEM micrograph of the substrate can be seen in Figure 1a (Philips EM-420, 36000×). Obviously, the substrate, including many of the holes, is highly covered by a network of catalyst and SWNTs. However, occasionally individual bundles longer than 1 μm can be observed bridging one of the holes (Figure 1c). The ends of those bundles are still connected to the network of catalysts and SWNTs that cover the carbon film, as can be seen in the magnified picture in Figure 1e (380000×). From this picture it is also clear that at least this particular SWNT bundle did not grow uniformly from a single catalyst but consists of at least two sub-bundles. This might be the reason for the possibility of mechanical disintegration of SWNT bundles by local AFM manipulation, as has recently been shown.[23]

Here we focus on the complementary Raman investigation of the same SWNT bundles that was performed with a home-built confocal microscope.[14,24] For a coarse approach, the sample is illuminated in the wide field mode where the position on the finder grid can be adjusted with a video camera. Then the microscope is used in the confocal mode where the sample is scanned through the diffraction limited excitation spot of the confocal microscope ($d \sim 350$ nm) and excited with a laser wavelength of $\lambda_{ex} = 514.5$ nm. The backscattered light passes a notch filter and is guided to spectrograph equipped with a charge coupled device (CCD) camera and, alternatively, with a point detector (avalanche photodiode, APD). For Raman imaging, the spectrograph is adjusted to the strong G-line $\pm$ 5 cm^{-1} in the Raman spectra (see below) of SWNTs, and the intensity is recorded at each position. This results in the "G-line images" of Figures 1b and 1d in which the free-standing individual SWNT bundles can be localized across the holes of the carbon film.

The main advantage of the investigation of free-standing tubes as compared to tubes that are deposited on a substrate is that there is essentially no background and also no surface interaction between the SWNTs and the substrate. For example, it has been shown that the same individual SWNT (bundles) can be investigated by Raman spectroscopy, AFM, and also TEM when the tubes are deposited on a thin (20 nm) Si_3N_4 membrane.[23] However, even though the membrane is highly transparent for the TEM beam, the background is still too high to identify the detailed structure of SWNTs, such as the tube walls within the bundles. Also, due to the strong intensity of the backscattered reflection and Rayleigh light from the substrate, the Raman spectra could only be obtained above 80−100 cm^{-1}. For the free-standing tubes on the other hand, the spectral range is only limited by the holographic notch filter and can be obtained down to 50 cm^{-1}.

A typical Raman spectrum of a free-standing bundle without any background subtraction is shown in Figure 2a. The main features are the RBMs at around 150 cm^{-1}, the D-line at 1350 cm^{-1}, and the G-line at 1590 cm^{-1}. While the frequency of the Raman bands is not changing after HRTEM investigation, the intensity decreases strongly. This is most likely due to the fact that, similar to chemical modification,[25] the electron bombardment in the TEM induces structural changes of the tubes and in turn reduces the Raman intensity.[26] Therefore the location of free-standing SWNTs was first investigated by low resolution TEM, which had no obvious effect on the Raman intensity. This was followed by the Raman experiments and finally by the HRTEM investigations.

The inset in Figure 2 shows a histogram of the observed RBM frequencies from 26 individual bundles. A Gaussian fit reveals a frequency distribution of 171 $\pm$ 9 cm^{-1}, which is in accordance with our previous experiments on purified

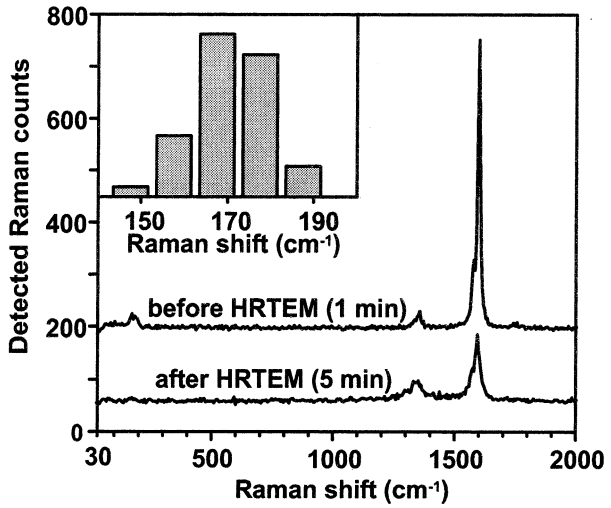

Figure 2. Raman spectra of free-standing bundles before and after HRTEM investigation at different acquisition times ($\lambda_{ex} = 514$ nm, $I = 500$ kW/cm^2). Inset: RBM frequency distribution $\omega_{RBM} = 171 \pm 9$ cm^{-1}.

SWNT material.[27] However, the frequency distribution cannot, in principle, be directly compared to the diameter distribution because not all of the tubes are excited to the same degree. In our Raman experiments, the signal can be detected only from individual tubes when the scattering process is resonantly enhancement, i.e., when the laser light has a similar energy as the absorbed or the scattered photon.[28] Here we used a laser wavelength of 514.5 nm, which is in resonance with the electronic transition energy of only semiconducting tubes within the given diameter distribution. In particular, it has been calculated that the resonance condition is fulfilled only for the E_{44}^S transition of nanotubes with a diameter between 1.9 and 1.5 nm and the E_{33}^S transition of tubes between 1.2 and 1.5 nm diameter.[17] Due to this enhancement selection, the detected Raman spectra result only from some of the tubes within a given bundle, which is of importance when comparing the RBM Raman frequencies and the tube diameters from TEM.

Here we investigated 26 isolated bundles with a thickness between 5 and 10 nm, i.e., a number of approximately 20−40 individual tubes each. Figure 3 shows a correlation of RBM spectroscopy and high resolution TEM for one of those bundles that did not show an aggregation of sub-bundles and was almost homogeneous over a length of a few hundred nanometers. In other words, the bundle structure did not change remarkably along the bundle segment that has been investigated complementarily by Raman spectroscopy.

From the TEM image in Figure 3a it can be seen that this particular bundle has a thickness of 7.5 nm. The parallel lines are assigned to the sidewalls of the SWNTs, because the mass density at the edge of the tube is higher than that in the center when the tube axis of the bundle is perpendicular to the incident electron beam. Therefore, the mean tube diameter can be approximately determined by the distance of the vertical lines.[10] The mean tube diameter from all bundles investigated was determined to be 1.46 ± 0.07 nm.

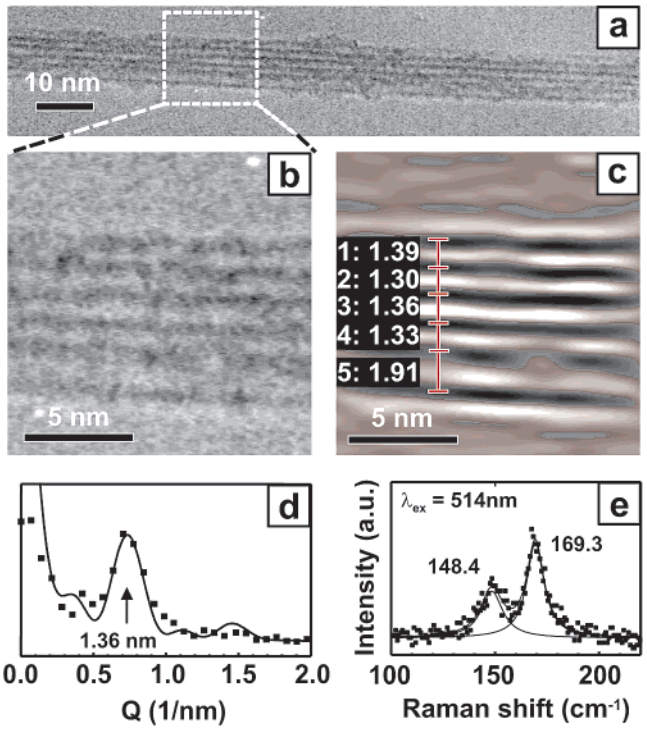

Figure 3. HRTEM images, data analysis and Raman spectra of a SWNT bundle. (a) HRTEM of an isolate bundle. The horizontal lines are assigned to the side walls of the SWNTs in the ordered bundle. (b) Magnified area of (a). (c) Fourier filtered image of (b) from which the "side wall distance" can be clearly determined. The values show the mean distance at several cross sections along the bundle shown in (a). (d) Fourier transform profile of (b) (dots) and fit function (solid line) indicating a mean "side wall distance" of 1.36 nm. (e) RBM range of the Raman spectrum from the same bundle as shown in (a). Two distinct Raman frequencies are strongly enhanced.

The mean tube diameter of the bundle segment enlarged in Figure 3b was determined from the profile of a Fourier transform of the image, which was fitted by the following scattering function:

$$I(Q) = I_0\left(\frac{\sin\pi bQ}{\pi bQ}\right)^2\left(\frac{\sin\pi NaQ}{\sin\pi aQ}\right)^2 \qquad (2)$$

Equation 2 describes the calculated intensity $I(Q)$ as a function of the width of the lines b, the number of lines N, and the line spacing a, which corresponds to the first maximum of the fit function. For the bundle segment shown in Figure 3b we calculated a mean line spacing of 1.36 nm. This is approximately the mean side wall distance (1−4) in the upper part of the bundle, as can be seen in the Fourier filtered image (Figure 3c). Actually, almost all of the investigated bundles showed a structure similar to the upper part in the HRTEM images in Figure 3. This makes sense because a TEM image shows only the projection of several tubes that are stacked on top of each other.

The diameter of an individual tube within the bundle can therefore be determined only if the tube is on the outer rim of the bundle, such as on the lower edges (5) of the bundle in Figure 3. In fact, this spacing (1.91 ± 0.15 nm) was the

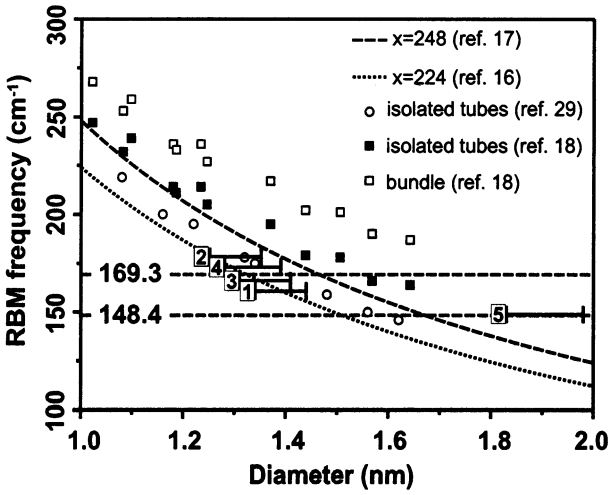

Figure 4. Diameter dependence of the RBM frequency as reported in the literature compared to the data of the bundle from Figure 3. The horizontal lines indicate the measured Raman frequencies, and the bars represent the accuracy of the measured "side wall distances" along the bundle (see also Figure 3). The group of distances around 1.35 nm (bars are offset for clarity) is tentatively assigned to the 169 cm^{-1} mode while the distance of 1.9 nm might belong to the frequency of 148 cm^{-1}.

largest side wall distance that could be observed in all samples investigated. At the same time, the corresponding Raman spectrum (Figure 3e) showed a band at 148.4 cm^{-1}, which was the lowest frequency that could be observed among the 26 individual bundles (left bar in Figure 2, inset). Therefore, there is a high possibility that the low-frequency component of the Raman spectrum belongs to the large tube diameter within the bundle. Consequently, the high-frequency component (169.3 cm^{-1}) would therefore belong to tubes within the group of distances between 1.3 and 1.4 nm.

The results for the bundle shown in Figure 3 are summarized in Figure 4 where we plotted the RBM frequency as a function of the tube diameter. In addition, we added the suggested RBM frequency dependence as calculated in refs 16 and 17 and several values calculated from force field and ab initio calculations for tubes with different diameter and chirality.[18,29] Assuming that the thicker tube within the bundle belongs to the lower energy vibration, we tentatively assign the corresponding bar to the 148.4 cm^{-1} mode which might result from a resonantly excited E_{44}^{S} transition of a relatively thick semiconducting tube. The band at 169.3 cm^{-1} would then belong to one or more tubes in the diameter range between 1.3 and 1.4 nm where the E_{33}^{S} transition is resonantly excited to gain the strong Raman signal.

Obviously, this direct correlation shows that the diameter dependence of the breathing mode frequency is well within the error of the expected values. However, for bundles of nanotubes with such a narrow diameter distribution, it is very complex to attribute small structural changes to distinct spectroscopic features. Therefore, so called "bundle effects" are experimentally very difficult to observe, even if single bundles are investigated with different microscopic techniques.

In summary, we have presented a method to directly correlate the structural and vibrational properties of bundles of carbon nanotubes. The use of substrates with a regular hole pattern allows to investigate the same free-standing bundles by high-resolution electron microscopy and Raman spectroscopy. We found that a direct comparison of the radial breathing mode frequency with the tube diameter obtained from TEM is difficult to establish from bundles of SWNTs because most of the bundles show a similar TEM pattern. Therefore, future work will focus on free-standing isolated tubes,[30] where an experimental correlation between diameter and vibrational frequencies could clearly be observed.

Acknowledgment. The authors thank Dr. Marko Burghard for valuable discussions and Prof. Thomas Basché for experimental support. This work was supported by the BMBF under contract No. 03C0302B9.

References

(1) Iijima, S. *Nature* **1991**, *354*, 56.
(2) Satio, R.; Dresselhaus, G.; Dresselhaus, M. S. *Physical Properties of Carbon Nanotubes*; Imperial College Press: London, 1998.
(3) Yenilmez, E.; Wang, Q.; Chen, R. J.; Wang, D.; Dai, H. *Appl. Phys. Lett.* **2002**, *80*, 2225.
(4) Postma, H. W.; Teepen, T.; Yao, Z.; Grifoni, M.; Dekker, C. *Science* **2001**, *293*, 76.
(5) Derycke, V.; Martel, R.; Appenzeller, J.; Avouris, Ph. *Nano Lett.* **2001**, *1*, 453.
(6) Journet, C.; Maser, W. K.; Bernier, P.; Loiseau, A.; de la Chapelle, M. L.; Lefrant, S.; Deniard, P.; Lee, R.; Fischer, J. E. *Nature* **1997**, *388*, 756.
(7) Thess, A.; Lee, R.; Nikolaev, P.; Dai, H.; Petit, P.; Robert, J.; Xu, C.; Lee, Y. H.; Kim, S. G.; Rinzler, A. G.; Colbert, D. T.; Scuseria, G. E.; Tománek, D.; Fischer, J. E.; Smalley, R. E. *Science* **1996**, *273*, 483.
(8) Ouyang, M.; Huang, J.; Cheung, C.-L.; Lieber, C. M. *Science* **2001**, *292*, 702.
(9) Amelinckx, S.; Lucas, A.; Lambin, P. *Rep. Prog. Phys.* **1999**, *62*, 1471.
(10) Qin, C.; Peng, L.-M. *Phys. Rev. B* **2002**, *65*, 155431.
(11) Henrard, L.; Loiseau, A.; Journet, C.; Bernier, P. *Eur. Phys. J. B* **2000**, *13*, 661.
(12) Yu, Z.; Brus, L. E. *J. Phys. Chem., B* **2001**, *105*, 6831.
(13) Dresselhaus, M. S.; Eklund, P. C. *Adv. Phys.* **2000**, *49*, 705.
(14) Mews, A.; Koberling, F.; Basché, Th.; Philipp, G.; Duesberg, G. S.; Roth, S.; Burghard, M. *Adv. Mater.* **2000**, *12*, 1210.
(15) Souza Filho, A. G.; Jorio, A.; Hafner, J. H.; Lieber, C. M.; Saito, R.; Pimenta, M. A.; Dresselhaus, G.; Dresselhaus, M. S. *Phys. Rev. B* **2001**, *63*, 241404.
(16) Bandow, S.; Asaka, S.; Saito, Y.; Rao, A. M.; Grigorian, L.; Richter, E.; Eklund, P. C. *Phys. Rev. Lett.* **1998**, *80*, 3779.
(17) Jorio, A.; Saito, R.; Hafner, J. H.; Lieber, C. M.; Hunter, M.; McClure, T.; Dresselhaus, G.; Dresselhaus, M. S. *Phys. Rev. Lett.* **2001**, *86*, 1118.
(18) Henrard, L.; Hernández, E.; Bernier, P.; Rubio, A. *Phys. Rev. B* **1999**, *60*, 8521.
(19) Milnera, M.; Kürti, J.; Hulman, M.; Kuzmany, H. *Phys. Rev. Lett.* **2000**, *84*, 1324.
(20) Venkateswaran, U. D.; Rao, A. M.; Richter, E.; Menon, M.; Rinzler, A.; Smalley, R. E.; Eklund, P. C. *Phys. Rev. B* **1999**, *59*, 10928.
(21) Rols, S.; Righi, A.; Alvarez, L.; Anglaret, E.; Almairac, R.; Journet, C.; Bernier, P.; Sauvajol, J. L.; Benito, A. M.; Maser, W. K.; Muñoz, E.; Martinez, M. T.; de la Fuente, G. F.; Girard, A.; Ameline, J. C. *Eur. Phys. J. B* **2000**, *18*, 201.
(22) Kuzmany, H.; Plank, W.; Hulman, M.; Kramberger, Ch.; Grüneis, A.; Pichler, Th.; Peterlik, H.; Kataura, H.; Achiba, Y. *Eur. Phys. J. B* **2001**, *22*, 307.
(23) Jiang, C.; Kempa, K.; Zhao, J.; Schlecht, U.; Kolb, U.; Basché, Th.; Burghard, M.; Mews, A. *Phys. Rev. B*, accepted.
(24) Koberling, F.; Mews, A.; Philipp, G.; Kolb, U.; Potapova, I.; Burghard, M.; Basché, Th. *Appl. Phys. Lett.* **2002**, *81*, 1116.

(25) Mews, A.; Jiang, C.; Schuessler, T.; Philipp, G.; Fan, Y.; Burghard, M. *Isr. J. Chem.* **2001**, *41*, 15.
(26) Smith, B. W.; Luzzi, D. E. *J. Appl. Phys.* **2001**, *90*, 3509.
(27) Zhao, J.; Jiang, C.; Fan, Y.; Burghard, M.; Basché, Th.; Mews, A. *Nano Lett.* **2002**, *2*, 823.
(28) Jorio, A.; Souza Filho, A. G.; Dresselhaus, G.; Dresselhaus, M. S.; Swan, A. K.; Ünlü, M. S.; Goldberg, B. B.; Pimenta, M. A.; Hafner, J. H.; Lieber, C. M.; Saito, R. *Phys. Rev. B* **2002**, *65*, 155412.
(29) Kürti, J.; Kresse, G.; Kuzmany, H. *Phys. Rev. B* **1998**, *58*, 8869.
(30) Kim, W.; Choi, H. C.; Shim, M.; Li, Y.; Wang, D.; Dai, H. *Nano Lett.* **2002**, *2*, 703.

NL025738O